Journal Name

ARTICLE TYPE

Cite this: DOI: 00.0000/xxxxxxxxxx

Amplified spontaneous emission in thin films of quasi-2D $BA_3MA_3Pb_5Br_{16}$ lead halide perovskites

Maria Luisa De Giorgi,*[a] Arianna Cretì,[b] Maria-Grazia La-Placa,[c] Pablo P. Boix,[c] Henk J. Bolink,[c] Mauro Lomascolo,[b] and Marco Anni[a]

Received Date
Accepted Date

DOI: 00.0000/xxxxxxxxxx

Quasi-2D (two-dimensional) hybrid perovskites are emerging as a new class of materials with high photoluminescence yield and improved stability compared to their three-dimensional (3D) counterparts. Nevertheless, despite their outstanding emission properties, few works have been reported on amplified spontaneous emission (ASE) and a thorough understanding of the photophysics of these layered materials is still lacking.

In this work, we investigate the ASE properties of multilayered quasi-2D $BA_3MA_3Pb_5Br_{16}$ films through the dependence of the photoluminescence on the temperature and provide a novel insight into the emission processes of quasi-2D lead bromide perovskites.

We demonstrate that the PL and ASE properties are strongly affected by the presence, above 190 K, of a minoritary fraction of high temperature (HT) phase. This phase dominates the PL spectra at low excitation density and strongly affects the ASE properties. In particular ASE is only present between 13 K and 230 K and, at higher temperature, it is suppressed by absorption of charge transfer states of the HT phase.

Our results improve the understading of the difficulties to obtain ASE at room temperature from these quasi-2D materials and are expected to guide possible materials improvement in order to exploit their excellent emission properties also for the realization of low threshold optically pumped lasers.

1 Introduction

Hybrid metal lead halide perovskites, such as $MAPbX_3$ (where MA=methyl ammonium and X=Cl, Br or I, or mixed Cl/Br and Br/I systems) are currently considered as an innovative and high-performance class of photovoltaic materials due to their large absorption coefficients, excellent charge mobility, and high diffusion lengths [1–11]. Thanks to the combination of the above-mentioned outstanding properties with the low-cost deposition process from solution, inexpensive solar cells, with certified power conversion efficiencies up to 25.2% [12], have been realized. Furthermore, these materials exhibit good light emission properties, that allow them to employ them as active materials for Light Emitting Diodes (LED) [13–20], Light Emitting Transistors [21] and Lasers [19,20,22–37]. For these reasons conventional tridimensional halide perovskites have recently undergone rapid development. Nevertheless, their instabilities over moisture, light, and heat remain a crucial challenge for the commercialization.

By contrast, the family of the layered 2D Ruddlesden-Popper-type perovskites, that are natural quantum well (QW) materials composed of layered perovskites between hydrophobic organic layers, have recently attracted increasing attention owing to their greater environmental stability, together with large exciton binding energy, strong quantum confinement effect and rapid decay rates making them very attractive for optoelectronic applications [38–42]

2D perovskites are formed by partially or fully replacing the cation (e.g., methylammonium - MA) with a larger one, thus modifying the 3D perovskite to a 2D layered structure due to steric hindrance [43], in which the inorganic layers of $[PbX_6]^{4-}$ are separated by sheets of larger organic cations giving rise to a multiple-quantum-well configuration where the inorganic layers represent the potential wells and the organic ones the barriers [44].

So the mixing of cations with different dimensions in the synthesis procedure results in layered perovskites with metal halide octahedral slabs of different thickness separated by the large organic cations. The obtained perovskites are generally defined by the number of n, that is the number of inorganic layers between two organic ones. In particular, n=1 corresponds to pure 2D structure and n=∞ to 3D.

The variation of the inorganic layer thickness (and conse-

[a] Dipartimento di Matematica e Fisica "Ennio De Giorgi", Università del Salento, Via per Arnesano, 73100 Lecce, Italy; E-mail: marialuisa.degiorgi@unisalento.it
[b] IMM-CNR Institute for Microelectronic and Microsystems, Via per Monteroni, 73100 Lecce, Italy.
[b] Instituto de Ciencia Molecular, Universidad de Valencia, Paterna, Valencia, 46980, Spain.

quently of the n-value), allows to modulate the quantum confinement within the wells, thus modifying the energy gap and the exciton binding energy that, in pure 2D materials can be as high as 400 meV, thus much higher than in the 3D materials[43,45].

The strongly bound excitons thus make 2D perovskites ideal for LEDs, LASERs and non-linear and polaritonic devices[43,46]. On the contrary, the high exciton binding energy limits the interconversion of excitons into free carriers and it is thus not ideal for efficient solar cells realization. Despite this, some results evidence that the exciton binding energy can be engineered in 2D perovskites by acting on the inorganic slabs thickness[47] or by realizing films with a vertical out-of-plane orientation with respect to the substrate surface[42], thus allowing the realization of solar cells with efficiency up to 12.52 %.

However, solution-processed 2D perovskites thin films generally are not in a single-phase, but consist of a set of mixed domains with different n-values, with multiple QW phases with different thickness coexisting in the films[48].

Ultrafast exciton funneling from high energy gap QWs ($n < 5$) to low energy gap ones ($n > 5$ to $n=\infty$), due to energy or charge transfer[44,48,49], has been demonstrated on the picosecond timescale (with near-unit efficiency) resulting, in large n-value domains, in improved efficiency of radiative recombination, overcoming the trap-mediated non-radiative one[50].

Moreover this ultrafast energy transfer leads to rapid accumulation of excitons in the wider QWs, thus potentially making easier to establish population inversion necessary for achieving ASE and lasing[51].

However, despite the exceptional emission features and the high efficiency of quasi 2D perovskites, very few experiments demonstrated to date optical gain and ASE in these materials. In particular even if bi-excitonic lasing was claimed in $(C_6H_{13}NH_3)_2PbI_4$ layered perovskite at low temperatures[52] already in 1998, the evidences of room temperature ASE have been to date very limited[53]. ASE was reported for $(PEA)_2MA_{(n-1)}Pb_nI_{(3n+1)}$ films, but only for n values of at least 12, but with a threshold increasing as n decreases, and much higher than the one of the corresponding 3D material[54].

Room temperature ASE in the green was also demonstrated, but only for proper alignment of the microcrystals of different dimensionality in the films[55] and tunable ASE was finally obtained in $(NMA)_2(FA)_{n-1}Pb_nX_{3n+1}$ [51].

In this work we investigate the photoluminescence and ASE properties of green emitting quasi-2D lead bromide perovskites ($BA_3MA_3Pb_5Br_{16}$) deposited by employing methylammonium (MA) and butylammonium (BA) as the small and large cations, respectively. In this material a PLQY exceeding 80% has been recently demonstrated[56], thus proposing it as interesting potential active material for light emitting devices, like LED and lasers.

We demonstrate ASE under nanosecond pumping from 13 K up to 230 K, with a progressively increasing threshold from 0.18 mJcm^{-2} to 5.8 mJcm^{-2}. The comparison between the PL spectra under high energy nanosecond pumping with standard spectra under weak excitation allows us to evidence that the sample emission is due to a single phase only between 13 K and 190 K, while at T $>$ 190 K the presence of a minoritary fraction of a second phase, which appears at high temperatures (HT), strongly affects the PL spectra and the ASE properties. In particular our results evidence the progressive suppression of ASE that can be ascribed to reabsorption from charge transfer states of the HT phase.

Our results improve the understanding of the processes competing with ASE at room temperature in quasi 2D perovskites and can be useful to develop engineered materials with improved ASE properties. Moreover the evidence of ASE in $BA_3MA_3Pb_5Br_{16}$ films represents a promising result encouraging further investigations to have a deep knowledge of the emission mechanism allowing the use of these innovative materials for laser applications.

2 Experimental section: materials and methods

2.1 Sample fabrication.

Thin films of quasi-2D $BA_3MA_3Pb_5Br_{16}$ perovskite, with thickness of about 200-230 nm, were prepared with the method reported in La-Placa et al.[56]. The perovskites precursor solution was prepared by dissolving BABr, MABr and PbBr2 in dimethyl sulfoxide (DMSO). The solution was stirred at 60 ºC overnight and was filtered using a PTFE syringe filter (0.22 μ) before deposition. The deposition on glass substrates was performed via a consecutive two-steps spin coating process at 1000 and 3000 rpm for 5 and 60 seconds, respectively. A solvent engineering process was carried out during the second spin-coating step by dripping 300 μL of chloroform onto the substrate.

2.2 Photoluminescence and Amplified Stimulated Emission measurements.

ASE properties have been explored by irradiating the films with a nitrogen laser at a wavelength of 337 nm delivering 3 ns pulses with a repetition rate of 20 Hz. The emission was collected by means of an optical fiber coupled to a spectrometer (ACTON SpectraPro-750) equipped with a Peltier cooled-CCD (Andor). The spectral resolution was about 0.5 nm.

In order to compare the ASE properties with the characteristic photoluminescence, PL experiments have been performed at low energy density exciting the samples by a solid state pulsed laser (mod. PLP-10, Hamamatsu), providing pulse of about 58 ps, at a wavelength of 400 nm, and at repetition rate of 1MHz. The maximum peak power was of about 70 mW, corresponding to an excitation density of about 1 μJcm^{-2} per pulse. The PL has been dispersed by an iHR320 (focal length of 0.32 m) Horiba monochromator equipped with a Peltier cooled Hamamatsu photomultiplier (Head-on mod R943-02), operating in single photon counting.

All the measurements were performed by collecting the signal, in waveguide configuration, from the edge of the film irradiated with the beam focused in a rectangular stripe (4mm x 80μm). Measurements have been performed in vacuum (pressure of about 10^{-2} mbar), at different temperatures in the range from 10 to 300 K, by using a closed cycle He cryostat.

3 Results and discussion

3.1 Amplified Spontaneous Emission.

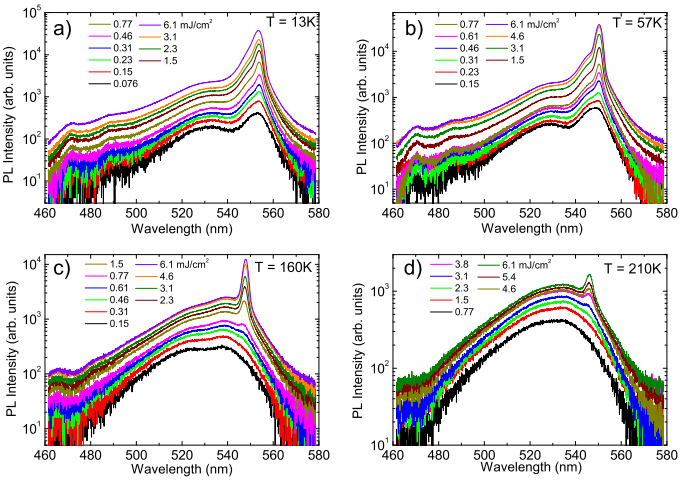

Fig. 1 PL spectra as a function of the excitation density at (a) T = 13 K, (b) T = 57 K, (c) T = 160 K and (d) T = 210 K, showing the gradual appearance of the ASE peak for increasing excitation density.

The ASE properties of the films have been investigated in the ns regime at different temperatures between T=13 K and room temperature by measuring the PL spectra as a function of the excitation density. As a first step we investigated the excitation density dependence of the spectra at T=13 K (see Fig. 1 a). At low excitation density the spectra show two weak peaks at about 473 nm and 489 nm, a broad peak at about 533 nm and a further narrower peak at about 552 nm. The obtained lineshape is comparable with the ones reported for similar systems in literature and allows us to ascribe the two peaks at lower wavelength to 2D domains with different values of n, and thus different thickness (likely n=2 and n=3). The $BA_3MA_3Pb_5Br_{16}$ structure has been confirmed by X-ray diffraction of the polycrystalline powder that is compatible with a low dimensional Ruddlesden-Popper perovskite phase with n close to 3 (see Fig. 2)[57]. Moreover the XRD analyses on the films indicate the same structure but with a lower size of the grains, suggested by the broadening of the diffraction peaks[56].

The peak at 533 nm in the PL spectra is blue-shifted of about 30 nm with respect to peak emission wavelength of 3D $MAPbBr_3$ (about 564 nm)[58], and it is thus ascribed to the exciton emission of thicker wells (FE in the following). Overall these features of the spectrum clearly evidence that the thin films contain domains with multiple QWs with different n-values.

Concerning the peak at 552 nm (LowE in the following) we observe that also this peak wavelength is not consistent with the $MAPbBr_3$ one, suggesting to ascribe it to the emission of low-energy edge-states due to the crystal disorder in the 2D domains[45,59].

We anyway observe that other possible attributions of the emission at low energy are present in literature[45,59,60] such as the distorsion of the perovskite octahedra, the exciton self-trapping, the dangling bonds, and the adsorption of molecules forming hybrid surface states. Moreover, since they are generally observed for n > 2 and their density increases with n, their origin could be due to those octahedral situated at the edge of the layers which are not in direct contact with the big organic spacers (BA cations in the case of our films)[59].

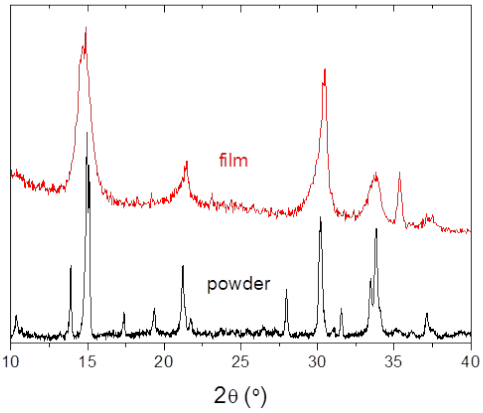

Fig. 2 X-ray diffraction patterns of $BA_3MA_3Pb_5Br_{16}$ polycrystalline powder and thin films.

By increasing the excitation density, a further peak centered at about 554 nm appears and its intensity grows rapidly with the excitation density. The excitation density dependence of the emission intensity at the new peak wavelength (see Fig. 3 a) allows to observe a clear slope increase in correspondence of the appearance of the peak in the spectra. This behavior is typical of the ASE process, and the value corresponding to the slope change represents the so-called ASE threshold, that is the smallest excitation density at which the ASE occurs[61].

The excitation density dependence of the PL spectra has been also investigated at higher temperatures (57 K, 160 K, 210 K). The obtained results (see Fig. 1 b-d) are qualitatively similar to the ones at 13 K, with the presence of the ASE peak at high excitation densities. Nevertheless, with the increase of the temperature, the ASE threshold value gradually increases (about 0.18, 0.27, 0.98 and 2.8 mJ/cm^2, for T=13 K, 57 K, 160 K and 210 K, respectively) and the ASE intensity decreases (see Fig. 3 a).

In order to investigate the origin of the observed ASE temperature dependence we acquired the spectra from 13 to 300 K at a fixed excitation density of 6 mJ/cm^2 (Fig. 3 b), about 2 times higher than the highest found threshold value. At each temperature we also determined the ASE threshold by continuously increasing the excitation density up to the beginning of lineshape variation due to the ASE peak appearance. The threshold has been thus estimated as the minimum excitation density allowing the observation of the ASE contribution to the PL spectrum.

The spectra at low temperatures show (see Fig. 3 b) clearly distinguishable peaks corresponding to the free exciton (FE), the LowE band and the ASE contribution. The different intensity temperature dependence of the FE and LowE bands and the increase of the linewidth makes the FE exciton peak and the LowE one progressively less distinguishable, while the ASE peak disappears

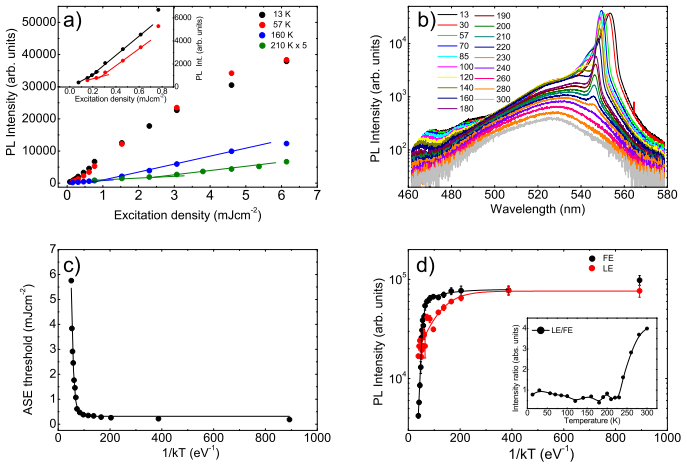

Fig. 3 a: Excitation density dependence of the emission intensity at the ASE peak wavelength at different temperatures. Inset: zoom of the region corresponding to the ASE threshold at 13 and 57 K. The lines are the best fit curves assuming a linear intensity increase below and above the ASE threshold, that clearly have different slope .b: Temperature dependence of the PL spectra at high excitation density (6 mJ/cm^2). c: Temperature dependence of the ASE threshold. The continuous line is the best fit curve. d: Temperature dependence of the FE (black dots) and LowE (red dots) peaks under ns-excitation. The lines are the best fit curves. Inset: temperature dependence of the LowE/FE relative intensity (the line is a guide for the eyes).

for temperatures above 230 K. The gradual worsening of the ASE efficiency is also well evidenced by the temperature dependence of the ASE threshold (see Fig. 3 c) showing a weak increase of about 2 times up to 140 K and then a strong increase up to 5.8 mJcm^{-2} at 230 K.

The individual intensity and peak wavelength of the three peaks have been determined from a best fit of the spectra with a multipeak function.

The temperature dependence of the FE and LowE peak intensities is reported in Fig. 3 d where we observe a weak temperature increase in the low temperature range, followed by an exponential quenching at higher temperatures.

This behaviour is typical of the thermal activation of non radiative processes, that can be reproduced by the following Arrhenius equation:

$$I(t) = \frac{I_0}{1 + \frac{\tau_i}{\tau_0} e^{-\frac{\Delta E}{k_B T}}} \quad (1)$$

where I_0 represents the integrated PL intensity for T= 0 K, ΔE is the activation energy, k_B is the Boltzmann constant, and τ_i and $\tau_0 e^{\frac{\Delta E}{k_B T}}$ are the radiative and the thermally activated non-radiative lifetime, respectively. It is straightforward to demonstrate that it comes from the steady state solution of the rate equation describing the exciton population:

$$\frac{dn}{dt} = g_0 - \frac{n}{\tau_i} - \frac{n}{\tau_0} e^{-\frac{\Delta E}{k_B T}} \quad (2)$$

A good agreement with the fit equation (see Fig. 3 d) is obtained for the LowE peak with a single activation energy of 19±2 meV (see Table 1) and a exciton lifetimes ratio $\frac{\tau_0}{\tau_i}$ of 6.2±1.2 (Table 2). On the contrary the FE exciton shows the contribution of two thermally activated processes. The first activation energy is of 17±10 meV, while the second is 130±20 meV (Table 1). The exciton lifetimes ratios are 0.62±0.30 and 2330±190, respectively (Table 2). The low activation energy is qualitatively consistent with the values found for the low energy PL peak in similar systems[53], suggesting a weak localization/binding energy of the edge states. The activation energy of the free exciton band quenching is instead of the typical order of magnitude of the exciton binding energy in 2D perovskites[62,63]. The difference in the $\frac{\tau_0}{\tau_i}$ values evidences a different relative importance of the temperature dependent and temperature independent relaxation decay times.

The clearly different intensity temperature dependence, activation energies, and exciton lifetimes ratios clearly confirms that these two peaks are due to radiative recombination of two different kind of emitters. The LowE/FE relative intensity (see inset of Fig. 3 d) is almost constant to about 0.7 up to 240 K and clearly increases up to 4 at room temperature. This result evidences that at room temperature the PL spectrum is dominated by the LowE emission (see Fig. 4 b).

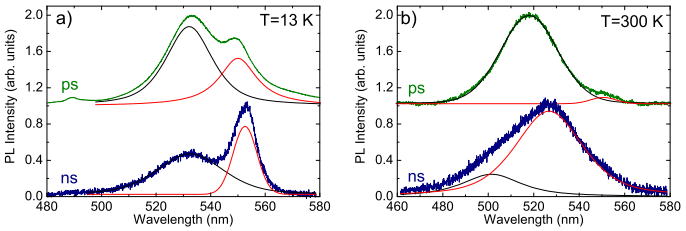

Fig. 4 Comparison of the PL spectra under ps (green line) and ns (blue line) at 13 K (a) and 300 K(b). The black and red peaks are the best fit of the FE and LE emission, respectively.

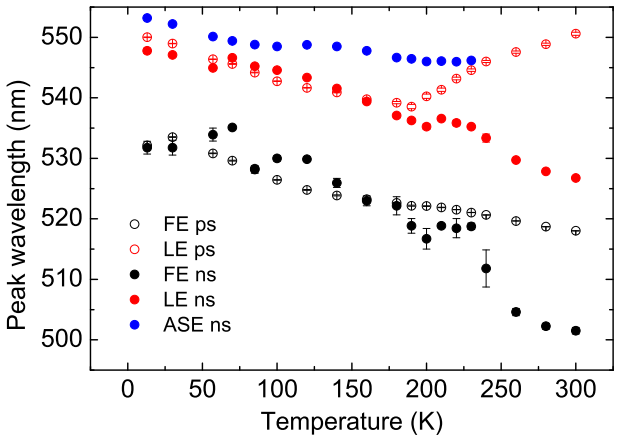

Fig. 5 Temperature dependence of the peak wavelength under nanosecond (filled dots) and picosecond (open dots) excitation regimes.

In order to quantitatively analyze the ASE threshold temperature dependence (Fig. 3 c) we observe that in case of excitonic emission our systems behaves as a three levels laser system, that is pumped at energy higher than the emission one, and efficiently relaxes from the pumped level to the emitting one. In this case,

in order to have positive gain, the population inversion has to be reached in the system, requiring to photogenerate a number of excitons of at least one half of the number of electrons in the top of the valence band, thus the threshold volumetric density of excitons n_{th} will be equal to N/2, where N is the volumetric density of electrons in the valence band top. Moreover the volumetric density of excitons can be easily related, in steady state condition, to the excitation density D, through the exciton lifetime τ, the sample absorption efficiency η_{abs}, the sample thickness d, the pump time length Δt and the pump photons energy $h\nu$ by the relation:

$$n = \frac{\eta_{abs} D \tau}{d h \nu \Delta t} \tag{3}$$

from which we can deduce the temperature dependence of the threshold excitation density D_{th}, assuming that both a radiative temperature lifetime, τ_i, and a non-radiative thermally activated lifetime, $\tau_0 e^{\frac{\Delta E}{k_B T}}$, contribute to the exciton relaxation:

$$D_{th} = \frac{N d h \nu \Delta t}{2 \eta_{abs}} \left(\frac{1}{\tau_i} + \frac{1}{\tau_0} e^{-\frac{\Delta E}{k_B T}} \right) = D_0 + D_1 e^{-\frac{\Delta E}{k_B T}} \tag{4}$$

Equation 4 predicts an ASE threshold increase with the temperature, consistent with the observed experimental behavior.

In order to fully reproduce the experimental ASE threshold temperature dependence (Fig. 3 c) two thermally activated non-radiative processes are required, with best fit values of the activation energies of ΔE_1 ~13.3±2.5 meV and ΔE_2 ~138±18 meV (see Table 1), thus in accordance with the values determined from the intensity temperature dependence of FE exciton band.

Finally, the temperature dependence of the three peak wavelengths, determined from the multipeak function best fit, has been plotted in Fig. 5 . We observe that the best fit values of both the FE exciton and LowE emission evidence a regular progressive blue-shift as the temperature increases.

Concerning the ASE peak (blue filled dots), we instead observe a blue shift similar to the one of the exciton and the LowE bands only up to 100 K. For higher temperatures between 100 K and 190 K a reduction of blue-shift is observed, followed by a temperature independent ASE wavelength up to the ASE disappearance above 230 K.

3.2 Temperature-dependence of the PL spectra.

In order to rationalize the origin of the observed ASE temperature dependence we also performed PL measurements under ps-pumping at low excitation density (about 1 μJcm^{-2}) in the range from 13 K to 300 K (see Fig.6 a).

The PL spectrum at 13 K (black curve in Fig.6 a), exhibits five distinct peaks: three weak peaks at about 446 nm (ascribed to n=1 QWs), 473 nm and 489 nm, respectively, a dominant PL peak at 533 nm and a further one at 549 nm, fully consistent with the n=2, n=3, FE and LowE peaks observed under nanosecond pumping. The similarity of the spectra under different excitation is also evident from the lineshape comparison (see Fig. 4 a), that evidences only a different FE/LowE relative intensity.

As the temperature increases we observe a progressive intensity decrease and a blue shift of the PL peak. Moreover we observe

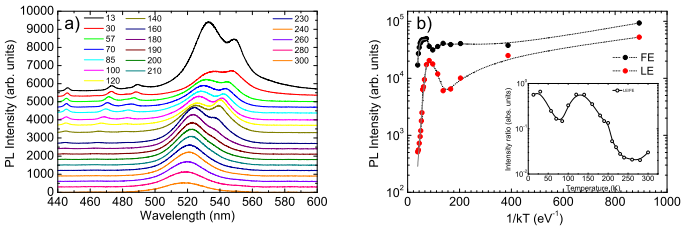

Fig. 6 a: PL spectra in the ps-regime as a function of the temperature. The curves are stacked vertically for sake of clarity. b: temperature dependence of the FE and LE intensity. The dotted lines are guide for the eyes, while the gray lines are the best fit curves. Inset: temperature dependence of the LE/FE relative intensity.

that the peak LowE becomes progressively less evident.

In order to explore in detail the PL temperature dependence, the exciton peak and the LowE one have been separated by fitting the PL spectra in the range 510-570 nm with a multipeak function (see Fig.4).

The temperature dependence of the two peak intensities (see Fig. 6 b) evidences that the FE exciton peak is dominant in all the temperature range, as also confirmed by the relative intensity temperature dependence (see inset of Fig.6 b). After an initial phase at low temperatures characterized by an interplay between the two peaks, an exponential decrease of the intensity, typical of the thermal activation of a non-radiative process, is observed for temperatures higher than 160 K for both peaks. In the same temperature range the relative intensity of LowE with respect to FE starts to significantly decrease from about 0.56 at 140 K, to just 0.02 at room temperature.

We observe anyway that, even if much weaker, the LowE peak is clearly visible in the spectra even at room temperature (see Fig. 4 b).

The activation energy of the exponential intensity decrease above 160 K has been determined through the best fit of the experimental intensities to Eq. 1. The best fit value of ΔE was 240± 20 meV and 142± 9 meV for the FE exciton and the LowE peaks, respectively (see Table 1), whereas the exciton lifetimes ratios $\frac{\tau_0}{\tau_i}$ for the FE exciton and the LowE peaks are of (178±8)10^2 and (20±8)10^3 (Table 2). They are interestingly different from the values obtained under ns excitation, suggesting that different states are involved in the emission.

Concerning the temperature dependence of the peaks wavelength we observe (see Fig. 5) the presence of two different regimes. Starting from 13 K the temperature increase leads to a progressive blueshift of both the FE exciton and the LowE bands, quantitatively very similar to the one observed under ns pumping, up to 190 K. For higher temperatures we instead observe a weaker blue shift for the FE exciton band and a clear shift inversion, from blue-shift to red-shift, of the LowE band. The inversion of the shift direction of the low energy band suggests that above 190 K this band is due to the emission from a state different from the LowE one, that we will call LowE$_2$ in the following.

Table 1 Activation energies inferred from the best fit procedure applied to the experimental data describing the temperature dependence of the FE, and LowE peak intensity and of the ASE threshold.

ACTIVATION ENERGIES			
Excitation regime	**ns regime** ΔE_1 (meV)	**ns regime** ΔE_2 (meV)	**ps regime** ΔE (meV)
LT phase			
LowE	19±2		
FE	17±10	130±20	
ASE threshold	13.3±2.5	138±18	
HT phase			
$LowE_2$			142± 9
FE			240±20

Table 2 Exciton lifetimes ratios from the best fit procedure applied to the experimental data describing the temperature dependence of the FE, and LowE peak intensity.

EXCITON LIFETIMES RATIOS τ_i/τ_0			
Excitation regime	**ns regime** (ΔE_1)	**ns regime** (ΔE_2)	**ps regime**
LT phase			
LowE	6.2±1.2		
FE	0.62±0.30	2330±190	
HT phase			
$LowE_2$			$(20\pm 3)10^3$
FE			$(178\pm8)10^2$

3.3 Discussion.

Overall our experimental results evidence that in the two different excitation regimes the emission originates from the same states only for low temperatures, up to 190 K, as evidenced by the good agreement of the peak wavelengths and the wavelength shift. A clearly different behaviour is instead observed above 190 K. The different temperature dependence of the two bands contributing to the sample emission under high energy density nanosecond pumping with respect to low excitation density ps determines a clear lineshape difference of the PL spectra at room temperature (see Fig. 4 b).

A plausible explanation of the observed trends is that at temperatures above 190 K two different pairs of emitting states are present in the films.

In particular, at 13 K the photoluminescence is likely due to excitons (FE) and low-energy edge-states (LowE) typical of the low temperature (LT) crystalline phase (represented in yellow in Fig.7) . As the temperature increases, both the states blueshift and at 190 K they intersect a "new pair" of states (in red in Fig. 7). At T>190 the two new states, characterized by an energy lower than the previous ones, dominate the PL emission at low excitation density (ps-regime). On the contrary, in the ns-regime, the peaks follow a regular trend suggesting that the emission always come from the same pair of states (LT states) (Fig. 7).

This behaviour suggests that the states dominating the ps PL have a low density (minority phase), and are thus saturated under much stronger nanosecond pumping, leading to a PL spectrum always dominated by the majority phase. The much lower excitation density used in the experiment with ps pumping instead allows to observe always the emission from the states at lower energy.

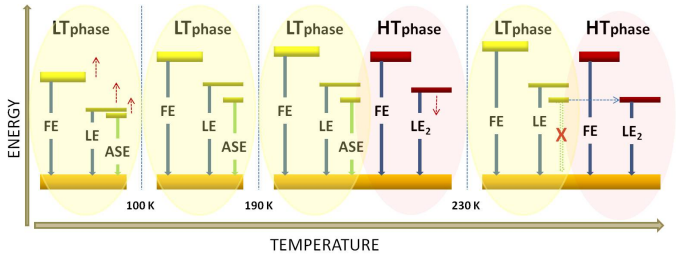

Fig. 7 Energy scheme of levels as function of the temperature

The observation of different emissive states with different density could be correlated to the well-known property of perovskites of changing the phase (by increasing the temperature). Our experimental data do not evidence a macroscopic phase variation, instead suggest the formation, at T > 190 K, of some domains of high temperature (HT) crystalline phase.

The presence of a minority fraction of domains of the HT phase is consistent with the recent report of existence, even at 4K, of domains of the high temperature phase in $(C_nH_{2n+1}NH_3)_2PbI_4$, despite a crystalline phase variation temperature of 270 K[64]. Further evidence of phase coexistence far from the macroscopic phase transition temperatures, ascribed to the interaction of nanostructured perovskites with the substrate, have been also reported in layered organic-inorganic perovskites[65] and in $CsPbBr_3$ NCs[66].

We thus ascribe the FE peak under ps excitation to free excitons of the low temperature (LT) phase up to 190 K and of the high temperature (HT) ones at higher temperature.

The $LowE_2$ state, visible above 190 K, shows a red-shift at higher temperature, not consistent with the emission from a state following the band gap. Furthermore it is worth to underline that the temperature range in which (in ps-regime) the $LowE_2$ peak inverts the shift perfectly coincides with the one is which the ASE shift slows down and the ASE intensity begins to decrease (see Fig. 5). Moreover the ASE disappears at the temperature at which energy of the peak $LowE_2$ matches the ASE peak energy.

These results clearly evidence that the ASE properties are affected by the temperature evolution of the peak $LowE_2$ and that, in particular, the $LowE_2$ state is in competition with the ASE. We tentatively ascribe $LowE_2$ peak to emission from charge transfer state of the HT phase. Indeed, since at 230 K the energy of the ASE level (in LT phase) and $LowE_2$ level (in HT phase) is very similar (Fig. 7), a process of charge transfer at the interfaces of different grains is highly probable. As a consequence, the spontaneous emission between the states in the HT phase is enhanced, while the ASE process is hindered. So the presence of the charge transfer state absorption limits the performances of these quasi-2D materials.

The observed competition between $LowE_2$ and ASE is fully consistent with the results on the ASE properties of

$(PEA)_2MA_{(n-1)}Pb_nI_{(3n+1)}$ suggesting the competition between ASE and a charge transfer state within the band gap, localized at the grain boundaries of the films[54].

We finally underline that the PL quenching from which we determined the activation energy of the FE and $LowE_2$ bands **(under ps pumping)** takes place in the temperature range in which the emission is due to the HT phase excitons and to the charge transfer states. So we ascribe the obtained activation energies to the binding energies of HT free exciton (240± 20 meV) and charge transfer states (142± 9 meV), respectively. This explains the difference with the values obtained under ns excitations.

Overall our results allow to conclude that ASE is present from the LT phase of the investigated samples, that dominates the PL spectra at high excitation density up to room temperature. However the ASE properties at temperatures above 190 K are significantly affected by the presence of the minority HT phase and of charge transfer states competing with the ASE.

4 Conclusion

Temperature-dependent PL measurements were performed in order to explore the emission properties of quasi-2D $BA_3MA_3Pb_5Br_{16}$ perovskite films. We demonstrated that the films are made of a mixture of wells with different thickness, even if most of the emission mainly originates from the thicker wells.

By analyzing the temperature-dependent PL spectra, two temperature regimes with different emission properties are identified, ascribed to the coexistence of HT and LT crystalline phases, dominating the PL spectra at low and high excitation density, respectively.

The quasi-2D $BA_3MA_3Pb_5Br_{16}$ perovskite shows ASE at low temperatures in the range 13-230 K, whereas at higher temperatures the ASE disappears, due to the competition between ASE and reabsorption from charge transfer states.

Conflicts of interest

In accordance with our policy on Conflicts of interest please ensure that a conflicts of interest statement is included in your manuscript here. Please note that this statement is required for all submitted manuscripts. If no conflicts exist, please state that "There are no conflicts to declare".

Author contributions

Conceptualization: MLDG; MA. Formal Analysis: MLDG; AC; ML; MA. Resources: MCLP; PPB; HJB. Supervision: MA. Writing – original draft: MLDG; MA. Writing – review editing: all the authors (MLDG; AC; MCLP; PPB; HJB; ML; MA). All authors have read and agreed to the published version of the manuscript.

Notes and references

1 H. J. Snaith, *Nat. Mater.*, 2018, **17**, 372–376.

2 S. D. Stranks and H. J. Snaith, *Nature Nanotechnol.*, 2015, **10**, 391.

3 M. B. Johnston and L. M. Herz, *Acc. Chem. Res.*, 2016, **49**, 146–154.

4 T. M. Brenner, D. A. Egger, L. Kronik, G. Hodes and D. Cahen, *Nat. Rev. Mater.*, 2016, **1**, 1–16.

5 M. Grätzel, *Nat. Mater.*, 2014, **13**, 838.

6 M. A. Green, A. Ho-Baillie and H. J. Snaith, *Nat. Photonics*, 2014, **8**, 506.

7 N.-G. Park, *J. Phys. Chem. Lett.*, 2013, **4**, 2423–2429.

8 H. Zhou, Q. Chen, G. Li, S. Luo, T.-b. Song, H.-S. Duan, Z. Hong, J. You, Y. Liu and Y. Yang, *Science*, 2014, **345**, 542–546.

9 W. Nie, H. Tsai, R. Asadpour, J.-C. Blancon, A. J. Neukirch, G. Gupta, J. J. Crochet, M. Chhowalla, S. Tretiak, M. A. Alam *et al.*, *Science*, 2015, **347**, 522–525.

10 Q. Dong, Y. Fang, Y. Shao, P. Mulligan, J. Qiu, L. Cao and J. Huang, *Science*, 2015, **347**, 967–970.

11 L. M. Herz, *ACS Energy Lett.*, 2017, **2**, 1539–1548.

12 *National Renewable Energy Laboratory.Research Cell Record Efficiency Chart (accessed July 30,2020)*, 2020, `https://www.nrel.gov/pv/cell-efficiency.html`.

13 N. K. Kumawat, X.-K. Liu, D. Kabra and F. Gao, *Nanoscale*, 2019, **11**, 2109–2120.

14 S. D. Stranks, V. M. Burlakov, T. Leijtens, J. M. Ball, A. Goriely and H. J. Snaith, *Phys. Rev. Appl.*, 2014, **2**, 034007.

15 H. Cho, S.-H. Jeong, M.-H. Park, Y.-H. Kim, C. Wolf, C.-L. Lee, J. H. Heo, A. Sadhanala, N. Myoung, S. Yoo *et al.*, *Science*, 2015, **350**, 1222–1225.

16 K. Lin, J. Xing, L. N. Quan, F. P. G. de Arquer, X. Gong, J. Lu, L. Xie, W. Zhao, D. Zhang, C. Yan *et al.*, *Nature*, 2018, **562**, 245–248.

17 Y. Cao, N. Wang, H. Tian, J. Guo, Y. Wei, H. Chen, Y. Miao, W. Zou, K. Pan, Y. He *et al.*, *Nature*, 2018, **562**, 249–253.

18 Q. Van Le, H. W. Jang and S. Y. Kim, *Small Methods*, 2018, **2**, 1700419.

19 S. A. Veldhuis, P. P. Boix, N. Yantara, M. Li, T. C. Sum, N. Mathews and S. G. Mhaisalkar, *Adv. Mater.*, 2016, **28**, 6804–6834.

20 B. R. Sutherland and E. H. Sargent, *Nat. Photonics*, 2016, **10**, 295.

21 X. Chin, D. Cortecchia, J. Yin *et al.*, *Nat. Commun.*, 2015, **6**, 7383.

22 G. Xing, N. Mathews, S. S. Lim, N. Yantara, X. Liu, D. Sabba, M. Grätzel, S. Mhaisalkar and T. C. Sum, *Nat. Mater.*, 2014, **13**, 476.

23 F. Deschler, M. Price, S. Pathak, L. E. Klintberg, D.-D. Jarausch, R. Higler, S. Hüttner, T. Leijtens, S. D. Stranks, H. J. Snaith, , M. Atatüre, R. T. Phillips and R. H. Friend, *J. Phys. Chem. Lett.*, 2014, **5**, 1421–1426.

24 M. L. De Giorgi and M. Anni, *Appl. Sci.*, 2019, **9**, 4591.

25 A. Balena, A. Perulli, M. Fernandez, M. L. De Giorgi, G. Nedelcu, M. V. Kovalenko and M. Anni, *J. Phys. Chem. C*, 2018, **122**, 5813–5819.

26 M. L. De Giorgi, A. Perulli, N. Yantara, P. P. Boix and M. Anni, *J. Phys. Chem. C*, 2017, **121**, 14772–14778.

27 M. L. De Giorgi, F. Krieg and M. Kovalenko, Maksym V.and Anni, *Sci. Rep.*, 2019, **9**, 17964.

28 M. L. De Giorgi, T. Lippolis, N. F. Jamaludin, C. Soci, A. Bruno and M. Anni, *J. Phys. Chem. C*, 2020, **124**, 10696–10704.

29 S. D. Stranks, S. M. Wood, K. Wojciechowski, F. Deschler, M. Saliba, H. Khandelwal, J. B. Patel, S. J. Elston, L. M. Herz, M. B. Johnston *et al.*, *Nano Lett.*, 2015, **15**, 4935–4941.

30 B. R. Sutherland, S. Hoogland, M. M. Adachi, C. T. Wong and E. H. Sargent, *ACS Nano*, 2014, **8**, 10947–10952.

31 J. Li, J. Si, L. Gan, Y. Liu, Z. Ye and H. He, *ACS Appl. Mater. Interfaces*, 2016, **8**, 32978–32983.

32 J. R. Harwell, G. L. Whitworth, G. A. Turnbull and I. D. W. Samuel, *Sci. Rep.*, 2017, **7**, 1–8.

33 S. Yakunin, L. Protesescu, F. Krieg, M. I. Bodnarchuk, G. Nedelcu, M. Humer, G. De Luca, M. Fiebig, W. Heiss and M. V. Kovalenko, *Nat. Commun.*, 2015, **6**, 8056.

34 P. Papagiorgis, A. Manoli, L. Protesescu, C. Achilleos, M. Violaris, K. Nicolaides, T. Trypiniotis, M. I. Bodnarchuk, M. V. Kovalenko, A. Othonos *et al.*, *ACS Photonics*, 2018, **5**, 907–917.

35 A. Dey, P. Rathod and D. Kabra, *Adv. Opt. Mater.*, 2018, **6**, 1800109.

36 S. A. Veldhuis, Y. K. E. Tay, A. Bruno, S. S. Dintakurti, S. Bhaumik, S. K. Muduli, M. Li, N. Mathews, T. C. Sum and S. G. Mhaisalkar, *Nano Lett.*, 2017, **17**, 7424–7432.

37 S. Chen, K. Roh, J. Lee, W. K. Chong, Y. Lu, N. Mathews, T. C. Sum and A. Nurmikko, *ACS Nano*, 2016, **10**, 3959–3967.

38 P. Acharyya, T. Ghosh, K. Pal, K. Kundu, K. Singh Rana, J. Pandey, A. Soni, U. V. Waghmare and K. Biswas, *Journal of the American Chemical Society*, 2020, **142**, 15595–15603.

39 P. Acharyya, K. Maji, K. Kundu and K. Biswas, *ACS Applied Nano Materials*, 2019, **3**, 877–886.

40 J. Xi, I. Spanopoulos, K. Bang, J. Xu, H. Dong, Y. Yang, C. D. Malliakas, J. M. Hoffman, M. G. Kanatzidis and Z. Wu, *Journal of the American Chemical Society*, 2020, **142**, 19705–19714.

41 P. Acharyya, K. Kundu and K. Biswas, *Nanoscale*, 2020, **12**, 21094–21117.

42 H. Tsai, W. Nie, J.-C. Blancon, C. C. Stoumpos, R. Asadpour, B. Harutyunyan, A. J. Neukirch, R. Verduzco, J. J. Crochet, S. Tretiak *et al.*, *Nature*, 2016, **536**, 312–316.

43 M. C. Gélvez-Rueda, E. M. Hutter, D. H. Cao, N. Renaud, C. C. Stoumpos, J. T. Hupp, T. J. Savenije, M. G. Kanatzidis and F. C. Grozema, *J. Phys. Chem. C*, 2017, **121**, 26566–26574.

44 Y. Chen, Y. Sun, J. Peng, J. Tang, K. Zheng and Z. Liang, *Adv. Mater.*, 2018, **30**, 1703487.

45 C. Zhao, W. Tian, J. Leng, Y. Zhao and S. Jin, *J. Phys. Chem. Lett.*, 2019, **10**, 3950–3954.

46 L. Zhang, Y. Liu, Z. Yang and S. Liu, *J. Energy Chem.*, 2019, **37**, 97 – 110.

47 J.-C. Blancon, A. V. Stier, H. Tsai, W. Nie, C. C. Stoumpos, B. Traore, L. Pedesseau, M. Kepenekian, F. Katsutani, G. Noe *et al.*, *Nature communications*, 2018, **9**, 1–10.

48 M. Yuan, L. N. Quan, R. Comin, G. Walters, R. Sabatini, O. Voznyy, S. Hoogland, Y. Zhao, E. M. Beauregard, P. Kanjanaboos *et al.*, *Nat. Nanotechnol.*, 2016, **11**, 872–877.

49 N. Wang, L. Cheng, R. Ge, S. Zhang, Y. Miao, W. Zou, C. Yi, Y. Sun, Y. Cao, R. Yang *et al.*, *Nat. Photonics*, 2016, **10**, 699–704.

50 Y. F. Ng, S. A. Kulkarni, S. Parida, N. F. Jamaludin, N. Yantara, A. Bruno, C. Soci, S. Mhaisalkar and N. Mathews, *Chem. Commun.*, 2017, **53**, 12004–12007.

51 M. Li, Q. Gao, P. Liu, Q. Liao, H. Zhang, J. Yao, W. Hu, Y. Wu and H. Fu, *Adv. Funct. Mater.*, 2018, **28**, 1707006.

52 T. Kondo, T. Azuma, T. Yuasa and R. Ito, *Solid State Commun.*, 1998, **105**, 253–255.

53 W. K. Chong, K. Thirumal, D. Giovanni, T. W. Goh, X. Liu, N. Mathews, S. Mhaisalkar and T. C. Sum, *Phys. Chem. Chem. Phys.*, 2016, **18**, 14701–14708.

54 M. R. Leyden, T. Matsushima, C. Qin, S. Ruan, H. Ye and C. Adachi, *Phys. Chem. Chem. Phys.*, 2018, **20**, 15030–15036.

55 R. Wang, Y. Tong, A. Manzi, K. Wang, Z. Fu, E. Kentzinger, J. Feldmann, A. S. Urban, P. Müller-Buschbaum and H. Frielinghaus, *Adv. Opt. Mater.*, 2018, **6**, 1701311.

56 M.-G. La-Placa, G. Longo, A. Babaei, L. Martínez-Sarti, M. Sessolo and H. J. Bolink, *Chem. Commun.*, 2017, **53**, 8707–8710.

57 C. C. Stoumpos, D. H. Cao, D. J. Clark, J. Young, J. M. Rondinelli, J. I. Jang, J. T. Hupp and M. G. Kanatzidis, *Chemistry of Materials*, 2016, **28**, 2852–2867.

58 H. C. Woo, J. W. Choi, J. Shin, S.-H. Chin, M. H. Ann and C.-L. Lee, *J. Phys. Chem. Lett.*, 2018, **9**, 4066–4074.

59 J.-C. Blancon, H. Tsai, W. Nie, C. C. Stoumpos, L. Pedesseau, C. Katan, M. Kepenekian, C. M. M. Soe, K. Appavoo, M. Y. Sfeir *et al.*, *Science*, 2017, **355**, 1288–1292.

60 J. Feng, C. Gong, H. Gao, W. Wen, Y. Gong, X. Jiang, B. Zhang, Y. Wu, Y. Wu, H. Fu, L. Jiang and X. Zhang, *Nat. Electron.*, 2018, **1**, 404–410.

61 S. Lattante, M. L. De Giorgi, M. Pasini and M. Anni, *Opt. Mater.*, 2017, **72**, 765–768.

62 D. B. Straus and C. R. Kagan, *J. Phys. Chem. Lett.*, 2018, **9**, 1434–1447.

63 N. Kitazawa, M. Aono and Y. Watanabe, *Mater. Chem. Phys.*, 2012, **134**, 875 – 880.

64 M. Baranowski, S. J. Zelewski, M. Kepenekian, B. Traoré, J. M. Urban, A. Surrente, K. Galkowski, D. K. Maude, A. Kuc, E. P. Booker, R. Kudrawiec, S. D. Stranks and P. Plochocka, *ACS Energy Lett.*, 2019, **4**, 2386–2392.

65 O. Yaffe, A. Chernikov, Z. M. Norman, Y. Zhong, A. Velauthapillai, A. Van Der Zande, J. S. Owen and T. F. Heinz, *Physical Review B*, 2015, **92**, 045414.

66 T. Whitcher, L. Gomes, D. Zhao, M. Bosman, X. Chi, Y. Wang, A. Carvalho, H. Hui, Q. Chang, M. Breese *et al.*, *NPG Asia Materials*, 2019, **11**, 1–12.